AAPS PharmSciTech (2024) 25:141
https://doi.org/10.1208/s12249-024-02858-y

RESEARCH ARTICLE

Development, Optimization, and *in vitro* Evaluation of Silybin-loaded PLGA Nanoparticles and Decoration with 5TR1 Aptamer for Targeted Delivery to Colorectal Cancer Cells

Seyyed Mobin Rahimnia[1,2] · Majid Saeedi[1,3] · Jafar Akbari[1] · Katayoun Morteza-Semnani[4] · Akbar Hedayatizadeh-Omran[5] · Rezvan Yazdian-Robati[3]

Received: 26 March 2024 / Accepted: 31 May 2024 / Published online: 19 June 2024

Abstract

Chemotherapeutic agents often lack specificity, intratumoral accumulation, and face drug resistance. Targeted drug delivery systems based on nanoparticles (NPs) mitigate these issues. Poly (lactic-co-glycolic acid) (PLGA) is a well-studied polymer, commonly modified with aptamers (Apts) for cancer diagnosis and therapy. In this study, silybin (SBN), a natural agent with established anticancer properties, was encapsulated into PLGA NPs to control delivery and improve its poor solubility. The field-emission scanning electron microscopy (FE-SEM) showed spherical and uniform morphology of optimum SBN-PLGA NPs with 138.57±1.30nm diameter, 0.202±0.004 polydispersity index (PDI), -16.93±0.45mV zeta potential (ZP), and 70.19±1.63% entrapment efficiency (EE). The results of attenuated total reflectance-Fourier transform infrared (ATR-FTIR) showed no chemical interaction between formulation components, and differential scanning calorimetry (DSC) thermograms confirmed efficient SBN entrapment in the carrier. Then, the optimum formulation was functionalized with 5TR1 Apt for active targeted delivery of SBN to colorectal cancer (CRC) cells *in vitro*. The SBN-PLGA-5TR1 nanocomplex released SBN at a sustained and constant rate (zero-order kinetic), favoring passive delivery to acidic CRC environments. The MTT assay demonstrated the highest cytotoxicity of the SBN-PLGA-5TR1 nanocomplex in C26 and HT29 cells and no significant cytotoxicity in normal cells. Apoptosis analysis supported these results, showing early apoptosis induction with SBN-PLGA-5TR1 nanocomplex which indicated this agent could cause programmed death more than necrosis. This study presents the first targeted delivery of SBN to cancer cells using Apts. The SBN-PLGA-5TR1 nanocomplex effectively targeted and suppressed CRC cell proliferation, providing valuable insights into CRC treatment without harmful effects on healthy tissues.

Keywords 5TR1 Aptamer · Colorectal cancer · PLGA nanoparticles · Silybin · Targeted delivery

✉ Majid Saeedi
majsaeedi@gmail.com

✉ Rezvan Yazdian-Robati
yazdianr921@gmail.com

1 Department of Pharmaceutics, Faculty of Pharmacy, Mazandaran University of Medical Sciences, Sari, Iran

2 Student Research Committee, Faculty of Pharmacy, Mazandaran University of Medical Sciences, Sari, Iran

3 Pharmaceutical Sciences Research Centre, Hemoglobinopathy Institute, Mazandaran University of Medical Sciences, Sari, Iran

4 Department of Medicinal Chemistry, Faculty of Pharmacy, Mazandaran University of Medical Sciences, Sari, Iran

5 Gastrointestinal Cancer Research Center, Non-Communicable Diseases Institute, Mazandaran University of Medical Sciences, Sari, Iran

Introduction

Colorectal cancer (CRC) is a prevalent type of cancer and is the second most common cause of cancer-related deaths in the United States. Research has shown that only 43% of CRC cases are detected in the early stages [1]. Conventional Chemotherapeutic agents such as 5-FU, which is widely used in the first-line treatment of CRC, often face significant limitations in their clinical application such as poor target specificity, leading to systemic toxicity and undesirable side effects. Additionally, developing multidrug resistance in cancer cells can render many chemotherapies ineffective over time [2, 3]. Surgery is the main treatment for CRC; however, a significant number (30-40%) have metastatic disease that cannot be treated with surgery [4]. Furthermore, CRC

patients face a high risk of cancer recurrence following treatment [5]. These limitations highlight the need to develop more targeted and effective drug delivery systems, such as PLGA nanoparticles (NPs), to improve the therapeutic index and patient outcomes [6].

Silybin (SBN), also known as Silibinin, is the major flavonolignan (50-70%) derived from Silymarin, a compound found abundantly in *Silybum marianum* (Milk thistle) fruit [7]. SBN is composed of two diastereomeric compounds (SBN A and SBN B) in a 1:1 ratio [8]. SBN has demonstrated significant anti-cancer properties in pre-clinical studies involving various epithelial cancers [9, 10]. Recently, dose-finding clinical trials of orally administrated SBN-phytosome were completed in prostate cancer [11, 12]. Additionally, a pilot study was conducted to obtain pharmacokinetic and pharmacodynamic information to aid the design of future CRC intervention studies with SBN, in CRC patients [10]. All these clinical trials have shown good tolerability and support its further application as a human CRC chemopreventive agent.

Several developments have been achieved in the past twenty years to enhance the therapeutic effectiveness of plant flavonoids, particularly in the treatment of cancer. However, the application of flavonoids such as SBN in anti-cancer therapy is hindered by factors including low bioavailability, poor flavonoid stability and solubility, and ineffective targeted delivery [13]. SBN is hindered by its low water solubility (0.4 mg/mL), leading to inadequate absorption and bioavailability when taken orally, which is the primary route of delivery for CRC patients. Pharmacokinetic studies have demonstrated that only 23-47% of SBN is absorbed from the gastrointestinal tract after oral administration [14]. Additionally, the low aqueous solubility of SBN may also contribute to difficulties in formulating stable and homogeneous drug preparations, further complicating its development as a CRC treatment. Therefore, to overcome these limitations appropriate drug delivery systems such as polymeric NPs would be beneficial. Nanotechnology has revolutionized therapeutic approaches by enabling the development of non-toxic cancer drug vehicles and controlled drug delivery using NPs [15, 16]. NPs can target cancer cells through active or passive mechanisms, leading to notable achievements in the development of targeted drug delivery systems aimed at enhancing treatment effectiveness [17, 18]. Various types of NPs have been developed for targeted drug delivery. The US FDA-approved PLGA stands out as a widely used and well-characterized biocompatible and biodegradable co-polymer. The PLGA copolymer is composed of varying ratios of lactic acid and glycolic acid monomer units, which can be tuned to achieve desired drug release kinetics [19, 20]. PLGA offers several advantages for cancer therapy, including an enhanced permeability and retention (EPR) effect, the ability to provide sustained and controlled drug delivery, enhanced accumulation of drugs in tumor vasculature, and targeted delivery by surface conjugation with targeting ligands such as peptides or aptamers (Apts) that can bind to specific targets, such as cancer cells or receptors. This approach can increase the effectiveness of treatment while reducing side effects [21–24]. NPs are characterized by their small size, which enhances their ability to interact with biological substrates. Size control is crucial and can be achieved by optimizing the preparation method. Preformed polymer-based methods are preferred due to their minimal toxic residues, unlike polymerization methods that may contain unreacted components. The choice of preparation method depends on the physicochemical properties of the polymer and drug. In this study, the emulsification-evaporation method, where a polymer is dissolved in a volatile solvent, was used to prepare SBN-loaded PLGA NPs [25, 26].

Apts are single-stranded DNA, RNA, or altered nucleic acid sequences that can bind to specific targets with high affinity. They are generated through the systematic evolution of ligands by exponential enrichment (SELEX) process [27]. Apts typically consist of 25-90 nucleotide bases and can fold into 3D complex structures that allow them to selectively bind to specific biomarkers. They are non-immunogenic, stable in various conditions, cost-effective, easy to synthesize, and have high specificity, making them valuable for applications in drug delivery, diagnosis, and bioimaging [28–30]. One well-studied Apt is the 5TR1 Apt which was specifically designed to bind tightly and selectively to the mucin 1 (MUC1) protein. This DNA Apt was first developed by Ferreira et al. MUC1 is a glycoprotein that serves as an upregulated tumor marker in various cancers, including stomach, lung, breast, prostate, colorectal, and others [31, 32].

In this study for the first time, we have developed SBN-loaded PLGA NPs and conjugated with 5TR1 Apt for targeted delivery of SBN to MUC1-positive CRC cells. Some preparation method variables were employed to optimize the SBN-loaded PLGA NPs according to their physicochemical properties. The optimization process aimed to identify the formulation with desirable characteristics such as particle size, polydispersity index (PDI), zeta potential (ZP), and drug encapsulation efficiency (EE). Furthermore, the optimum formulation was selected to conjugate covalently 5TR1 Apt using a carbodiimide coupling agent, in case of active targeting. The efficacy of this targeted delivery nanovehicle, comprising the SBN-loaded PLGA NPs conjugated with the 5TR1 Apt, was then evaluated through a series of *in vitro* experiments. These analyses assessed the targeted delivery and anticancer activity of the developed nanocomplex against MUC1-positive CRC cells.

Materials and Methods

Materials

SBN ($C_{25}H_{22}O_{10}$) was provided by Exir company (Wien, Austria). PLGA acid terminated (Mw:7000–17.000Da, lactide: glycolide=50:50), N-hydroxy sulfosuccinimide (NHS), 1-ethyl-3-(3-dimethylaminopropyl) carbodiimide hydrochloride (EDC), and MTT were obtained from Sigma Aldrich. RPMI 1640 medium, fetal bovine serum (FBS), penicillin-streptomycin (Pen/Strep), and trypsin-EDTA (0.25%) were bought from Gibco (Darmstadt, Germany). Tween 80 was purchased from Merck, Germany. The 5TR1 DNA Apt, 5′-GAAGTGAAAATGACAGAACACAACA-3′ amino was synthesized by Microsynth AG (Balgach, Switzerland). Human colorectal adenocarcinoma cell line (HT29), murine colorectal carcinoma cell line (C26), and Chinese hamster ovary cell line (CHO) were obtained from the Pasteur Institute of Iran (Tehran, Iran).

SBN-Loaded PLGA NPs Preparation

SBN-loaded PLGA NPs were synthesized using a previously published modified single emulsion evaporation technique [33–35]. In brief, 10 mg of PLGA and 1 mg of SBN were dissolved in 2 mL of acetone. The resulting solution was then added to an aqueous phase of Tween 80 (1% w/v) and sonicated on ice (amplitude 50%, 5 min) using a probe sonicator (Bandelin, Germany). To evaporate the organic solvent, the reaction was continued while stirring overnight. Centrifugation (21000 rpm, 25°C, 30 min) produced the NPs, which were then washed to remove excess surfactant and free SBN and then lyophilized to produce powder. In this study, a series of experiments were conducted with different process parameters to optimize the SBN-loaded PLGA NP formulation. The parameters investigated included the drug-to-polymer ratio and the concentration of the surfactant Tween 80. These specific parameters were selected based on the findings of previous studies similar to the current work [36–41]. The researchers aimed to examine the effects of these variables on the critical quality attributes of the NPs, including the EE%, mean particle size (Z-average, nm), PDI, and ZP (mV). The optimization of these process parameters was a crucial step in the development of the targeted nanodelivery system, as the physicochemical characteristics of the NPs can significantly influence their performance in terms of drug encapsulation, colloidal stability, and targeting efficiency.

Particle size, PDI, and ZP Measurement

The Malvern Zetasizer equipment and DTS software were used for analyzing the particle size (nm), PDI, and ZP (mV) of SBN-PLGA NPs [42]. To perform this, 1 mg of synthesized NPs were dispersed in 1mL of deionized water and sonicated to create a homogenous dispersion. Then three independent measurements were done.

Entrapment Efficiency Measurement

SBN encapsulation was measured using Knauer HPLC equipment. The HPLC system was outfitted with a Knauer C18 column, which had a particle size of 5µm and dimensions of 4.6×250mm, an isocratic pump, and a UV/vis detector. The mobile phase of 10:90% (v/v) water/methanol was supplied at a flow rate of 0.7 $mL.min^{-1}$. SBN encapsulation content was measured by dissolving freeze-dried SBN-PLGA NPs in acetonitrile and filtering them through a 0.22-µm PTFE syringe filter. Chromatograms were recorded at 288nm with a 20µL injection volume at a temperature of 25°C. The calibration curve employed standard solutions containing SBN in acetonitrile at concentrations of 5, 10, 20, 40, 80, and 100 µg. mL^{-1} [43].

$$EE\% = \frac{amount\ of\ SBN\ in\ NPs}{amount\ of\ SBN\ in\ formulation} * 100$$

Limit of Detection and Limit of Quantification for HPLC

The limit of detection (LOD) and limit of quantification (LOQ) were determined using the following mathematical equations:

$$LOD(\mu g/mL) = 3.3\sigma/S$$

$$LOQ(\mu g/mL) = 10\sigma/S$$

Here, σ represents the standard deviation of the lowest concentration and S represents the slope of the calibration curve.

Morphological Investigation using the Field-Emission Scanning Electron Microscopy (FE-SEM)

The optimum SBN-PLGA NPs had been stored for 24 hours at -80 °C. Through the freeze drier Alfa 1-2Id Plus (Martin Christ GmbH, Germany) all items were lyophilized. FESEM (TESCAN-MIRA3, Czech Republic) morphological examinations of the optimum formulation were verified on samples coated with a thin gold film [44].

Attenuated Total Reflectance-Fourier Transform Infrared (ATR-FTIR) Spectroscopy

ATR-FTIR studies were performed for SBN, PLGA, Tween 80, the freeze-dried blank PLGA NPs (without drug), and

the freeze-dried optimum SBN-PLGA formulation. ATR-FTIR spectra were recorded between 4000-650 cm^{-1} with 2 cm^{-1} of resolution using a Cary 630 FTIR spectrometer (Agilent Technologies Inc., CA, US) with a diamond ATR [45].

Differential Scanning Calorimetry (DSC) Analysis

DSC (Perkin Elmer, Netherlands) was applied to show DSC traces for each ingredient in the SBN-PLGA formulation. Five mg of SBN, PLGA, the freeze-dried blank PLGA NPs, and the freeze-dried optimal SBN-PLGA NPs were weighed, placed in aluminum pans, and sealed hermetically. The samples underwent examination at a heating rate of 10 °C/min under a nitrogen atmosphere, ranging from 30 to 300 °C [46].

Stability Studies

The stability of the lyophilized optimum SBN-PLGA NPs (F5) was assessed at 4 and 25 °C for three months in a well-closed container and dark place, by ICH (International Council for Harmonization) guidelines. Physical stability was examined which included the effects of temperature and time on size (nm), ZP (mV), EE%, and PDI after rehydration [47].

Conjugation of 5TR1 Apt on the Surface of NPs

About 1 mL (10 mg/mL) of PLGA–SBN NPs suspension in DNase/RNase-free water was treated with 400 mmol/L of EDC and 100 mmol/L of NHS. The mixture was incubated at room temperature with moderate shaking for 1 hour. The resultant NHS-activated particles were rinsed with DNase/RNasee-free water to eliminate any residual NHS or EDC, then centrifuged (15 minutes, 1500g). Activated SBN-PLGA NPs were covalently bonded to 100µL of 3' NH2 modified 5TR1 Apt at room temperature for 18 hours, with regular mixing. To eliminate any free Apt, a 15-minute centrifugation at 1500 g was used [32, 48]. To evaluate the efficiency of 5TR1-nanocomplex formation, gel electrophoresis, and UV-spectrophotometry methods were performed [15, 49].

In vitro Drug Release Test

The release of SBN from SBN-PLGA-5TR1 nanocomplex was determined using the direct addition method by measuring the cumulative amount of SBN released from the nanocomplex over a periodic time interval. Lyophilized SBN-PLGA-5TR1 nanocomplex (1mg/mL) was placed into a 2-mL microtube and dispersed in two separate release media including phosphate buffer saline pH 7.4 (containing 0.1% w/v tween 80) and citrate buffer pH 5.5 (0.1 M citric acid and 0.1 M sodium citrate solution containing 0.1% w/v tween 80). The microtubes were placed in a shaker incubator at 37°C under constant shaking. At various intervals (1, 2, 4, 6, 8, 24, 48, 72, 96, 120, and 144 hours), one microtube of each pH was removed and centrifuged (13000g, 4°C, 20 min), the supernatant was filtered through a 0.22-µm membrane filter and analyzed with HPLC instrument at 288nm [50–52]. Then the cumulative percent of SBN released from the nanocomplex was calculated. The test was done in triplicate.

Kinetic Analysis of the Release Data

Different kinetic models, including zero order, first order, Higuchi diffusion, and Korsmeyer-Peppas, were used to match the *in vitro* release data to provide insight into the release kinetics of the formulations. The model with the greatest r^2 value was selected as the most plausible explanation [53].

Cell Culture

HT29, C26 (MUC1-positive CRC cell lines), and CHO (as normal cell line) were cultured in RPMI medium supplemented with 10% (v/v) FBS and 1% (v/v) Pen/Strep solution. The cells were incubated at 37 °C in a humidified environment with 5% (v/v) CO_2 [54].

In vitro Cytotoxicity Assay

HT29, C26, and CHO cells were seeded in 96-well cell culture microplates at a density of 7×10^3 cells/100 µL. Following 24 hours, the cells were exposed to a range of concentrations of free SBN (10-500 µM), blank PLGA NPs, SBN-PLGA NPs, and SBN-PLGA-5TR1 nanocomplex, incubated for 48 h. For the completion of the procedure, 10 µL of fresh MTT reagent (final concentration 0.5 mg/mL) was introduced to each well and remained for 4 hours in the incubator. The MTT reagent was subsequently discarded, and the purple formazan crystals were dissolved in dimethyl sulfoxide (DMSO). The sample's absorbance was measured at 570nm using a microplate (ELISA) reader (BioTek, Winooski, Vermont, US) [55–57].

$$\text{Surveillance}\ (\%) = \left[OD_{570}(\text{sample})/OD_{570}(\text{control})\right] * 100$$

Cell Apoptosis Evaluation

To detect early and late apoptosis, a total of 100,000 cells/well were placed in a 24-well plate (n=3) and exposed to free SBN, SBN-PLGA NPs, and SBN-PLGA-5TR1 nanocomplex for 48 hours. The Apoptosis kit from Mahboub

Bio Research in Tehran, Iran was used to assess distinctions between normal and apoptotic cells after the procedure. The kit includes annexin V-FITC (20 µg/ml), 1x binding buffer, and propidium iodide (PI, 50 µg/ml). The cells were washed with phosphate-buffered Saline (PBS) and then exposed to 500 µL of 1× binding buffer containing 2 µL of the annexin V solution for 15 minutes in a dark environment at room temperature. Following this, 1 µL of the PI solution was introduced and incubated for an additional 5 minutes. After incubation, cells were observed via the Partec PAS flowcytometer instrument (Sysmex Partec GmbH company, Münster, Germany). The utilization of annexin V-FITC when combined with PI, a red fluorescent chemical that binds to DNA, but is not taken up by living cells, enables the distinction of necrotic cells [58].

Statistical Assessments

The study utilized several statistical tests to evaluate the outcomes. Specifically, the researchers employed a 2-tailed Student's t-test and a one-way Analysis of Variance (ANOVA) to compare the means between groups. The Student's t-test is a commonly used test to determine if the difference in means between two groups is statistically significant. The one-way ANOVA was used to compare the means across multiple groups. After the ANOVA, the Tukey-Kramer post-hoc test was conducted to identify which specific group means differed significantly. All statistical analyses were performed using GraphPad Prism version 7. The data were presented as the mean ± standard deviation (SD), and the experiments were replicated a minimum of three times, as stated in the text. A p-value less than 0.05 was considered statistically significant.

Results

The Effect of Drug: Polymer Ratio on

To optimize SBN-loaded PLGA NPs various drug: polymer ratios (1:1, 1:2, 1:5, and 1:10 w/w) were investigated. The other formulation parameters were kept constant and Tween 80 concentration was 1% w/v (Table I).

Particle Size of SBN-PLGA NPs

As shown in Table I the mean hydrodynamic diameter values of NPs were determined using the z-average diameter or intensity-weighted average size measured with dynamic light scattering (DLS). As the drug: polymer ratio increased from 1:1 (F1) to 1:10 (F5), a remarkable increase in particle size from 57.14±3.65 to 138.57±4.30 nm was observed (*P<0.0001*).

PDI of SBN-PLGA NPs

A decrease in the drug: polymer ratio from 1:1 to 1:10 w/w led to a reduction in PDI from 0.425 to 0.202 (*P>0.05*), which implies a narrow size distribution.

ZP of SBN-PLGA NPs

The ZP value was -10.12±0.21mV while the drug: polymer proportion was high (1:1 w/w), but when the proportion was reduced to 1:10 w/w, the ZP became more negative (-16.93±0.45mV), which implies an increase in the repulsive force between NPs (*P<0.0001*).

The Effect of Tween 80 Concentration on

In this study, we used four different concentrations (0, 1, 2, and 5% w/v) of Tween 80 in the aqueous phase, maintaining a consistent drug: polymer ratio of 1:10.

Particle Size of SBN-PLGA NPs

Increasing Tween 80 concentration from 1% to 5% w/v led to a significant rise in SBN-PLGA NPs size, from 138.57±1.30nm to 181.40±1.28nm (*P<0.0001*).

PDI of SBN-PLGA NPs

Table I showed increasing Tween 80 from 1% to 5% w/v led to an unremarkable increase in PDI which may be due to the particle growth (*P>0.05*).

ZP of SBN-PLGA NPs

The F4 formulation, which lacked Tween 80, displayed the lowest ZP (-7.74±0.75), leading to NP attraction and instability. Furthermore, increasing Tween 80 from 1% to 5% w/v resulted in a significant reduction in negative ZP from -16.93±0.45 to -10.67±0.99mV (*P<0.001*).

Drug Entrapment Efficiency

The drug EE% of all SBN-PLGA NPs made with different drug: polymer ratios and Tween 80 concentrations were presented in Table I. Among all the batches, F5 with an EE% of 70.19±1.63% was selected for further studies. The effect of the drug: polymer ratio on EE% was investigated, revealing a significant increase from 41.02±1.73% to 70.19±1.63% as the ratio decreased from 1:1 to 1:10 (increasing PLGA amount) (*P<0.001*). The effect of Tween 80 concentration on the EE% was evaluated. As indicated in Table I, elevating Tween 80 from 1% to 5% w/v resulted in a notable decrease in the EE% of SBN from 70.19% to 46.84% (*P<0.01*).

SBN-PLGA-5TR1 conjugation

According to Table I, conjugation of F5 with 5TR1 Apt led to an increase in particle size and ZP to 149.33±2.152nm and -21.44±0.671mV, respectively, with unremarkable impact on PDI value and EE% of SBN-PLGA NPs. Due to the negative charge of the Apt molecule, ZP of F5 exhibited a more negative value.

LOD and LOQ calculation for HPLC analysis

According to the standard curve equation (y=192373x+147128, R^2=0.999) and SD of the lowest concentration (349.77, after three analyses) the LOD and LOQ obtained were calculated as 0.006 µg/mL and 0.018 µg/mL, respectively. Hence, the proposed method is sensible for SBN analysis in pharmaceutical formulations and might be useful to determine drug release kinetics from the PLGA NPs matrix.

Morphological Study of the Optimized Formulation

F5 was selected as the optimum formulation for FESEM microscopy as shown in Figure 1. The image reveals that all SBN-PLGA NPs are well separated, exhibiting spherical shapes and relatively uniform sizes.

ATR-FTIR Spectra

Figure 2 displays the ATR-FTIR spectra of the original materials, the freeze-dried blank PLGA NPs, and the optimized SBN-PLGA NPs (F5). The ATR-FTIR spectrum of SBN exhibited the characteristic peak at 3456 cm^{-1} (O-H stretching), 3150-3050 cm^{-1} (aromatic C-H stretching), 3000-2850 cm^{-1} (aliphatic C-H stretching), 1633 cm^{-1} (C=O stretching), 1600-1467 cm^{-1} (aromatic C=C stretching), and 1300-1000 cm^{-1} (C-O stretching) that is in agreement with previous studies [59]. The ATR-FTIR spectrum of PLGA displayed the main peaks at 3650-3450 cm^{-1} (O-H stretching), 3000-2850 cm^{-1} (aliphatic C-H stretching), 1746 cm^{-1} (C=O stretching), and 1300-1000 cm^{-1} (C-O stretching) [60]. The ATR-FTIR spectrum of Tween 80 showed the major peaks at 3502 cm^{-1} (O-H stretching), 2922 cm^{-1} (-CH_2 asymmetric stretching), 2859 cm^{-1} (-CH_2 symmetric stretching), 1735 cm^{-1} (C=O stretching), and 1093 cm^{-1} (C-O stretching) [42].

DSC Thermogram

The DSC experiment was conducted on existing forms of the pure SBN, PLGA, Tween 80, the freeze-dried blank PLGA NPs, and SBN-PLGA NPs (Figure 3). The DSC of the 50:50 PLGA sample revealed thermal alterations associated with the glass transition of the polymer occurring within a temperature range of 48 to 56 °C, with a midpoint at 52 °C [61]. The DSC thermograms show the presence of an endothermic peak in the DSC trace of silybin, as seen in Figure 4. The DSC peak reached its maximum at a temperature of 172 °C, which closely aligns with the documented melting point of SBN. A modest endothermic peak was seen after the main peak, which occurred at around 180 °C. This peak might be attributed to impurities [37].

Stability Studies

The stability examination was performed over three months at temperatures of 4 and 25 °C, using ZP, EE%, particle size, and PDI as indicators (Table II).

Formation of SBN-PLGA-5TR1 Nanocomplex

The gel electrophoresis experiment was used to demonstrate the formation of the SBN-PLGA-5TR1 nanocomplex [62]. In lane C, it was seen that the movement of the 5TR1 Apt band was completely prevented when employing the EDC/NHS linker, and the band corresponding to the free Apt disappeared. This is in contrast to the weak band observed in lane E, which showed a small amount of free Apts present in the sample (Figure 4). In lane D (SBN-PLGA NPs) a weak shininess is related to the PLGA excitation by UV light. The second experiment examined the existence of Apt on NPs by UV spectroscopy and evaluated the effectiveness of conjugation [63]. The UV absorbance of DNA at 260 nm on the PLGA NPs that underwent the conjugation process with 5TR1 Apt was 0.398±0.007 and 0.103±0.004 in the presence and absence of EDC/NHS, respectively (the blank sample was plain PLGA NPs). So, a higher quantity of Apts was attached to NPs in the presence of the linkers. These findings suggest that the interaction between 5TR1 Apt and the SBN-PLGA NPs was significantly enhanced by the catalysts, resulting in a strong and covalent bond between the Apts and the NPs.

In vitro Drug Release Behavior and Kinetic

Figure 5 displays the cumulative percentage release profile of SBN from F5-5TR1 nanocomplex at two different pH values. Both at pH 5.5 and 7.4, a slow and sustained release of SBN from PLGA NPs was observed, lasting for 144 hours at a temperature of 37±0.5 °C. There was a considerably high percentage of drug release (92.319±1.269%) over 144 hours in pH 5.5 compared to the neutral physiologic pH=7.4 (25.410±0.642%). We observed zero order release patterns at pH=5.5, with a maximum r^2 value of 0.9975 (y=0.5482x+12.796).

Table I Characteristics and compositions of formulations. The dataset includes the mean±SD for three repeated measurements

Formulation	SBN [a] (mg)	PLGA (mg)	Tween 80 (mg)	Acetone (mL)	Water up to (mL)	SBN/PLGA ratio	Particle size (nm)	PDI [b]	ZP [c] (mv)	EE [d] (%)
F1	1	1	100	2	10	1:1	57.14 ± 3.65	0.425 ± 0.011	-10.12 ± 0.21	41.02 ± 1.73
F2	1	2	100	2	10	1:2	89.23 ± 3.73	0.417 ± 0.009	-13.07 ± 0.30	53.02 ± 2.93
F3	1	5	100	2	10	1:5	109.17 ± 1.78	0.231 ± 0.015	-15.67 ± 0.40	64.00 ± 1.46
F4	1	10	0	2	10	1:10	855.32 ± 5.81	0.781 ± 0.022	-7.74 ± 0.75	Unstable
F5	1	10	100	2	10	1:10	138.57 ± 1.30	0.202 ± 0.004	-16.93 ± 0.45	70.19 ± 1.63
F6	1	10	200	2	10	1:10	163.80 ± 2.30	0.215 ± 0.006	-13.33 ± 0.75	52.82 ± 0.92
F7	1	10	500	2	10	1:10	181.40 ± 1.28	0.226 ± 0.003	-10.67 ± 0.99	46.84 ± 7.28
F5-5TR1 *	1	10	100	2	10	1:10	149.33 ± 2.15	0.208 ± 0.038	-21.44 ± 0.67	70.32 ± 2.03

(a) Silybin, (b) Polydispersity Index, (c) Zeta Potential, and (d) Entrapment Efficiency. *: The optimum SBN-PLGA formulation (F5)-conjugated with 1 µM of 5TR1 solution

Cell Cytotoxicity Evaluations

The proliferation of CRC cells (C26 and HT29) and normal CHO cells, which are MUC1 positive and MUC1 negative cells respectively, were tested using colorimetric MTT assays (Figure 6). Initially, investigations were conducted to examine the effects of different doses of SBN (ranging from 0 to 300 µM), revealing a reduction in cellular viability with increasing SBN concentrations. The IC_{50} values of SBN for CHO, C26, and HT29 cells were 173.38, 174.01, and 158.85 µM, respectively, after 48 hours of incubation. The CHO cells exhibited greater viability (84.88±1.51%) when incubated with SBN-PLGA-5TR1 nanocomplex, in comparison to free SBN (56.84±3.26%) (*P<0.001*). After 48 hours of treatment with SBN-PLGA, C26, and HT29 cell viability was 59.97±3.43% and 66.31±6.64%, respectively, which decreased significantly to approximately 40.90±0.86% (*P<0.001*) and 34.01±3.43% (*P<0.0001*), respectively after treatment with SBN-PLGA-5TR1 nanocomplex (Fig. 7).

Annexin V-FITC/Propidium Iodide Apoptosis Assay

This analysis aimed to identify the cause of the proliferation inhibitory mechanism seen in SBN-PLGA NPs, SBN-PLGA-5TR1 nanocomplex, and free SBN solution (Figure 8). The green fluorescence of Annexin V-FITC and the red fluorescence of PI were detected through the FL1 and FL3 channels, respectively. The graph is partitioned into four quadrants (Q), where Q1 represents necrotic cells, Q2 and Q4 represent late and early apoptotic cells, respectively, and Q3 indicates viable cells. The proportion of cells in the Q4 quadrant, representing cells in the early stage of apoptosis, increased to 27.11% and 25.27% for C26 and HT29, respectively, after exposure to SBN-PLGA-5TR1 nanocomplex. The percentage of cells in the Q2 phase of late apoptosis rose to 12.22% and 7.58% in C26 and HT29 cells, respectively, after treatment with SBN-PLGA-5TR1 nanocomplex. Between the treatment groups on CHO cells, just free SBN have necrotic and late apoptosis mechanisms with 20.89 and 16.41%, respectively and the other groups had no significant impact on the cell's proliferation.

Discussion

The SBN-PLGA NPs were formulated using the single emulsion evaporation process, with Tween 80 used as a surfactant. The impact of processing factors such as the drug: polymer ratio and the percentage of surfactant on size, PDI, ZP, and EE% of the NPs was investigated (Table I).

According to the results, a significant rise in particle size was observed with a further increase in PLGA quantity (decreasing drug: polymer ratio), which could be attributed

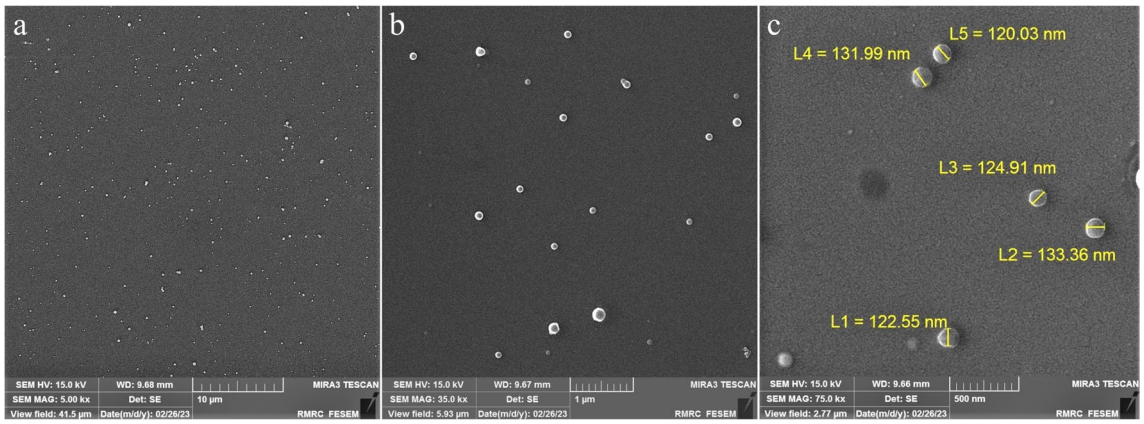

Fig. 1 FESEM images of optimum SBN-PLGA NPs (F5). **a** x5000, **b** x35000, and **c** x75000 magnifications

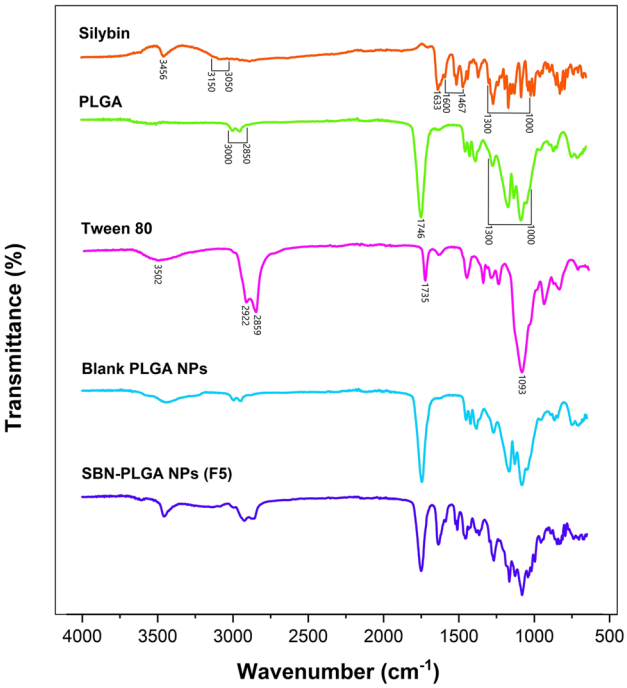

Fig. 2 ATR- FTIR spectra of pure Silybin, PLGA polymer, Tween 80, freeze-dried blank PLGA NPs, and freeze-dried SBN-PLGA NPs (F5)

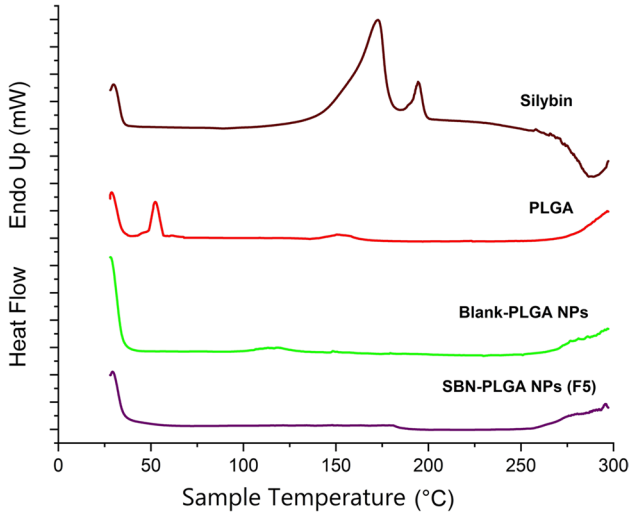

Fig. 3 The DSC thermogram of Silybin, PLGA, freeze-dried blank PLGA NPs, and freeze-dried SBN-PLGA NPs (F5)

to the limited availability of surfactant (Tween 80) to regulate particle size [64]. The same result has been reported by Tripathi et al. The particle size of the NPs exhibited a drastic increase as the drug-to-polymer ratio was decreased. Specifically, the NPs size increased from 430 nm to 920 nm when the drug-to-polymer ratio was decreased from 1:1 to 1:4 (w/w). One possible explanation for this phenomenon is the rising viscosity of the PLGA solution. As the polymer concentration increased, the higher viscosity of the solution led to inadequate dispersibility into the aqueous phase during the NPs formation process [36].

Studies have shown that using Tween 80 as an emulsifier, instead of Tween 20 or Tween 40, results in improved NPs characteristics, regardless of their concentrations. This improvement is likely due to Tween 80's superior emulsification capacity, which helps stabilize the NPs during the formulation process. The concentration of Tween in the aqueous phase also plays a crucial role in determining NPs size [65].

Higher Tween 80 concentrations can lead to a significant increase in the NP's diameter. This effect is believed to be related to the surfactant packing parameters, as described by the critical packing parameter (P_c) theory proposed by Mitchell and Ninham and calculated using a specific equation [40, 66, 67]:

$$P_c = v/a_{0.}l_c$$

a_o: the effective head group area, v: the volume of the hydrophobic tail, and l_c: the extended length of the tail in the core of the micelle.

The P_c parameter is critical for predicting shape and dimensions. The SBN-PLGA NPs size was increased at higher concentrations of Tween 80 due to enhanced hydration of head groups (a_o), which decreases the P_c, leading to the formation of larger emulsion droplets [40]. Despite Span, increasing Tween 80 reduces P_c, enlarges NPs due to its PEO chains, and increases viscosity, yielding highly aggregated droplets. This hinders ultrasonication and stirring, detrimentally increasing NPs size [68].

The PDI score ranges from 0 to 1, and a formulation that is monodisperse and homogenous should provide values around zero. PDI values over 0.7 indicate very polydisperse NPs, while values below 0.5 indicate homogenous NPs and will be suitable for further work [69, 70]. According to these data, decreasing the drug: polymer ratio from 1:1 to 1:10 w/w resulted in an unremarkable decrease in the size distribution index. The preparation with the highest PLGA content had the lowest PDI value. The presence of more acid-terminated PLGA molecules could lead to higher negative charges (ZP), decreasing the aggregation tendency of NPs, improving dispersion, and minimizing the PDI value. The preparation without Tween 80 (F4) exhibited the greatest PDI value and led to instability and precipitation. Yuan et al. found that PLGA NPs prepared with Tween 80 exhibited a smaller average size and a narrower PDI compared to the PLGA NPs without Tween 80. Tween 80 provides steric stability, preventing particle aggregation, and potentially serving as an emulsifier resulting in decreased particle size with more uniformity [37].

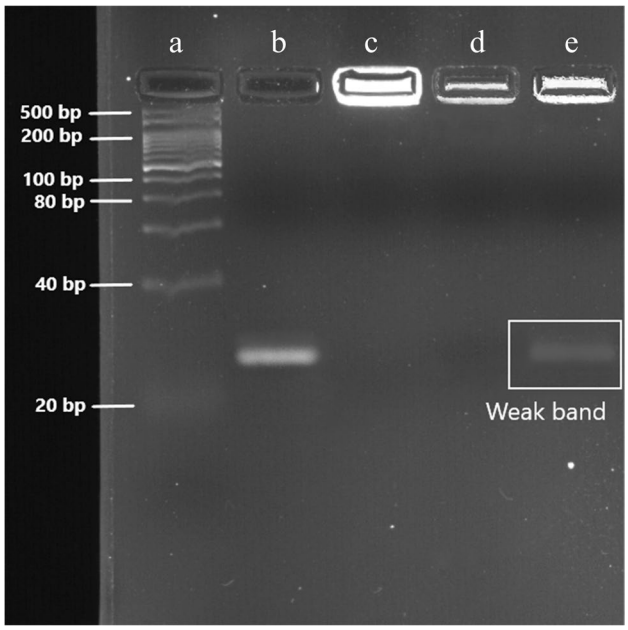

Fig. 4 Gel electrophoresis image. Lane **a** 500 bp DNA ladder, Lane **b** free 5TR1 Apt; Lane **c** SBN-PLGA NPs reacted with 5TR1 in the presence of linker (5TR1-nanocomplex), Lane **d** SBN-PLGA NPs, and Lane **e** SBN-PLGA NPs reacted with 5TR1 in the absence of linker

The ZP is a measure of the electric charge present on the shear plane of particles in a colloidal system. It serves as an indicator of the system's physical stability. Charged particles (more than ±10 mV) are often less prone to particle aggregation because of the repulsive force caused by electric charges [71]. Higher negative values of ZP were obtained for SBN-PLGA NPs due to the presence of terminal carboxyl groups in the polymer followed by increasing PLGA concentration. Xie et al. reported similar results, where increasing the PLGA concentration from 4% to 16% w/v decreased zeta potential to more negative values significantly [72]. Moreover, with a rise in the ZP, the repulsive contact will become stronger, resulting in the creation of NPs that are more stable and have a more consistent distribution of sizes [73]. The reduction of ZP with Tween 80 enhancement occurred because the carboxylic groups of PLGA couldn't undergo esterification in the aqueous medium, leading to a reduction in carboxylate (COO-) production, which carries a negative charge. The presence of non-ionic surfactants such as polysorbates on NPs surface diminishes electrophoretic mobility, thus reducing the ZP [74].

Similar to our findings a study examining the PLGA concentration effect (2, 5, and 10 %) on estradiol EE% also found that as polymer concentration enhanced, particle size

Table II Stability data for the chosen SBN-PLGA NPs (F5) after being stored for 3 months and rehydration (data are shown as mean±SD, n=3).

Storage conditions	Time (month)	Particle size (nm)	PDI	ZP (mV)	EE%
Initial	0	138.57±1.30	0.202±0.004	-16.93±0.45	70.19±1.63
4°C	1	138.99±1.15	0.204±0.008	-16.87±0.42	69.85±1.10
	2	139.12±1.20	0.206±0.005	-16.99±0.39	69.35±2.02
	3	139.78±2.01	0.208±0.011	-17.00±0.60	69.09±1.78
25°C	1	139.39±2.17	0.205±0.006	-17.22±0.64	69.06±3.10
	2	140.00±3.00	0.206±0.012	-17.20±0.51	69.00±2.46
	3	140.58±1.99	0.211±0.021	-18.01±0.36	68.89±2.88

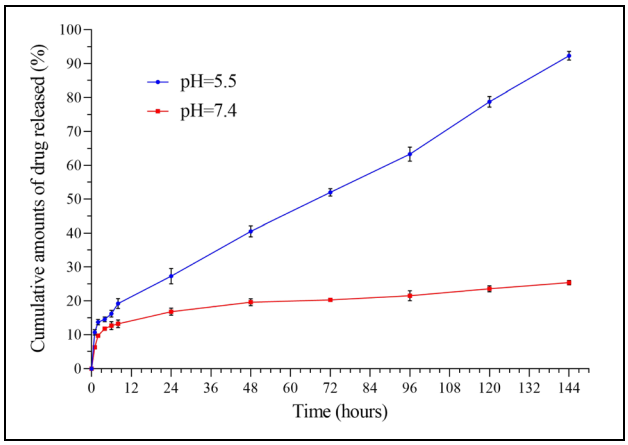

Fig. 5 The SBN release profile from the F5-5TR1 nanocomplex in two different pH conditions. Data are shown as mean±SD (n= 3). The difference was statistically significant ($P<0.05$)

and EE% of estradiol increased considerably. This is attributed to the expanding polymeric matrix's ability to entrap more hydrophobic drug molecules like estradiol and SBN [38]. The EE% decline with Tween 80 elevation might be due to the surfactant's solubilizing effect, potentially enhancing SBN solubility in the aqueous phase and drug leakage from the polymeric matrix. Additionally, exceeding the critical micelle concentration (CMC) of Tween 80 causes the migration of Tween 80 molecules from the interface (nanodroplet surface), leading to a decrease in the EE% [39, 41]. Consequently, Tween 80 properties were altered in high concentrations, leading to its inability to maintain the emulsion during the production of NPs [75].

The findings suggest that the most effective drug: polymer ratio and Tween 80 concentration for achieving the highest quality SBN-PLGA formulation is 1:10 w/w and 1% w/v, respectively (F5). The F5 formulation exhibited a significantly higher drug EE% of 70%, the highest ZP of -17 mV, and the lowest PDI value of 0.202, indicating a homogeneous and potentially stable preparation for further analyses. Additionally, its small particle size of 138 nm rendered it a suitable vehicle for drug delivery of SBN to CRC cells through passive targeting. NPs with sizes below 200 nm efficiently internalize by cells through endocytosis and the EPR effect of tumor vasculature [76].

According to the FESEM analysis, the NPs were spherical and monodisperse with particle size close to the DLS results (Figure 1). The slight difference in size between the DLS and FESEM results can be attributed to several factors. The measurement technique is one of the most important factors that affect size variation. DLS measures the hydrodynamic size of particles and provides an average size based on the *Brownian* motion, while FESEM directly images the size of individual particles using an electron beam leading to more precise measurement [77]. The effect of NPs shape on the interactions between NPs and cell membranes has also been examined by various groups. Interestingly, it was reported that the cellular uptake quantity of spherical NPs was five times higher than rod-like NPs through endocytosis [78]. Therefore, the prepared SBN-PLGA NPs can penetrate the CRC cells more easily because of their spherical shape.

ATR-FTIR spectroscopy is an effective method for indicating probable chemical interactions between drugs and polymers (Figure 2). According to the ATR-FTIR findings, there was no chemical interaction between SBN and the other materials in the chosen formulation, since the C=O stretching peak of SBN can be detected in the ATR-FTIR spectrum of the F5 formulation without shifting in wavenumber. The ATR-FTIR analysis indicated that SBN was

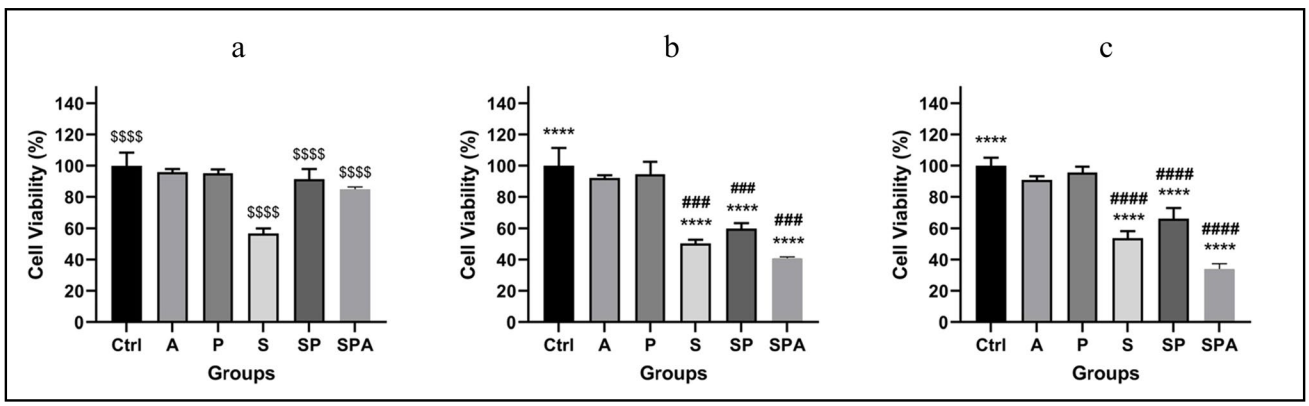

Fig. 6 MTT assay of treatment groups in three cell lines after 48 hours. **a** Treatment in CHO cell line, **b** Treatment in C26 cell line, and **c** Treatment in HT29 cell line. The treatment groups were Ctrl: Negative control (without treatment), a A: Free 5TR1, P: Blank PLGA NPs, S: Free SBN, SP: SBN-PLGA NPs (F5), and SPA: SBN-PLGA-5TR1 (F5-5TR1) nanocomplex. The dose of SBN in all treatment groups was constant based on the IC_{50} of free SBN in each cell line. **** $P<0.0001$ in comparison to the negative control, $^{###}$ $P<0.001$ and $^{####}$ $P<0.0001$ in comparison to the SPA group, and $^{\$\$\$\$}$ $P<0.0001$ in comparison to the S group. Data are shown as mean±SD (n=5)

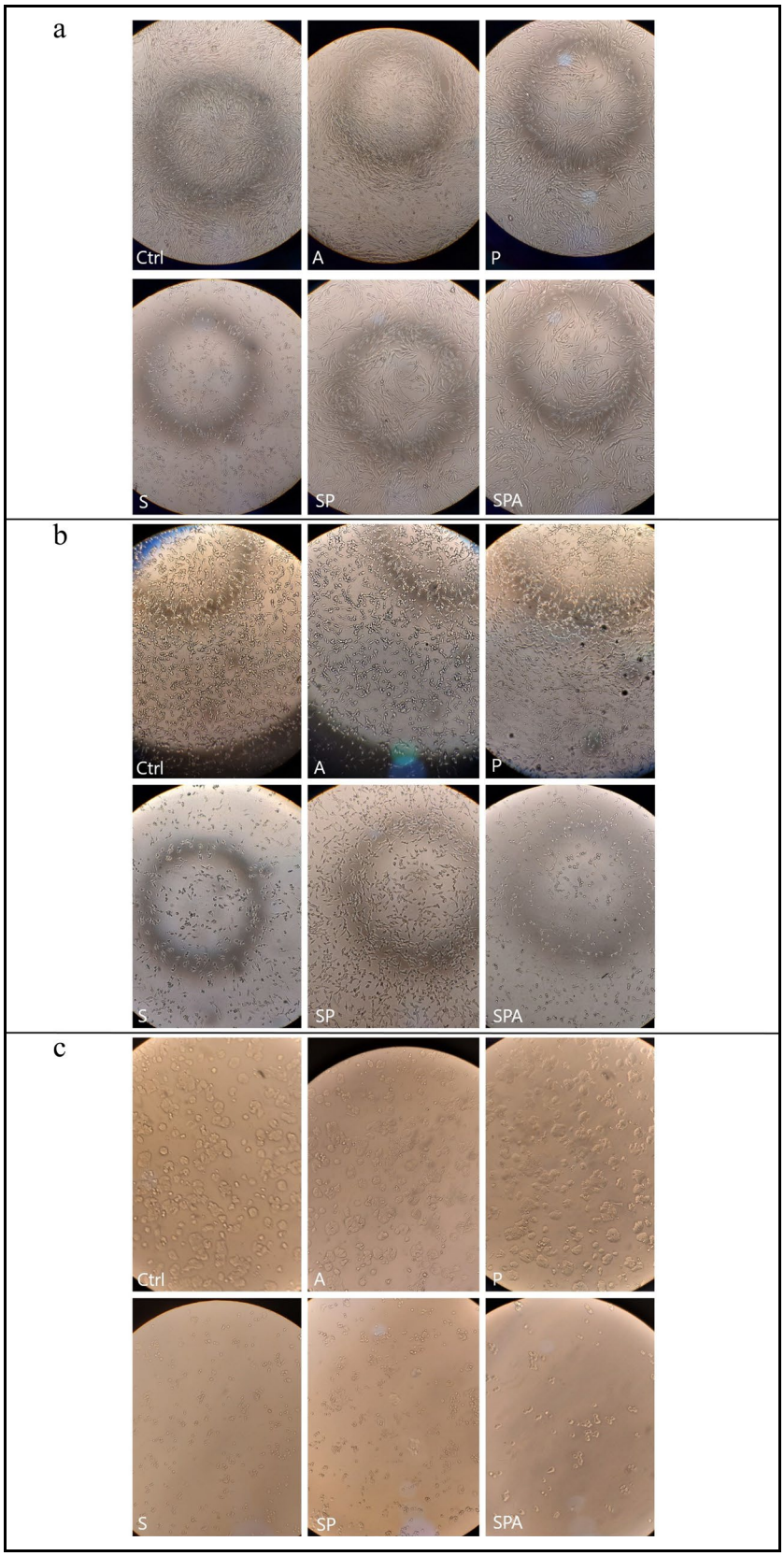

Fig. 7 Cell images of MTT assay. **a** Treatment in CHO cell line, **b** Treatment in C26 cell line, and **c** Treatment in HT29 cell line. The treatment groups were Ctrl: Negative control (without treatment), A: Free 5TR1, P: Blank PLGA NPs, S: Free SBN, SP: SBN-PLGA NPs (F5), and SPA: SBN-PLGA-5TR1 (F5-5TR1) nanocomplex

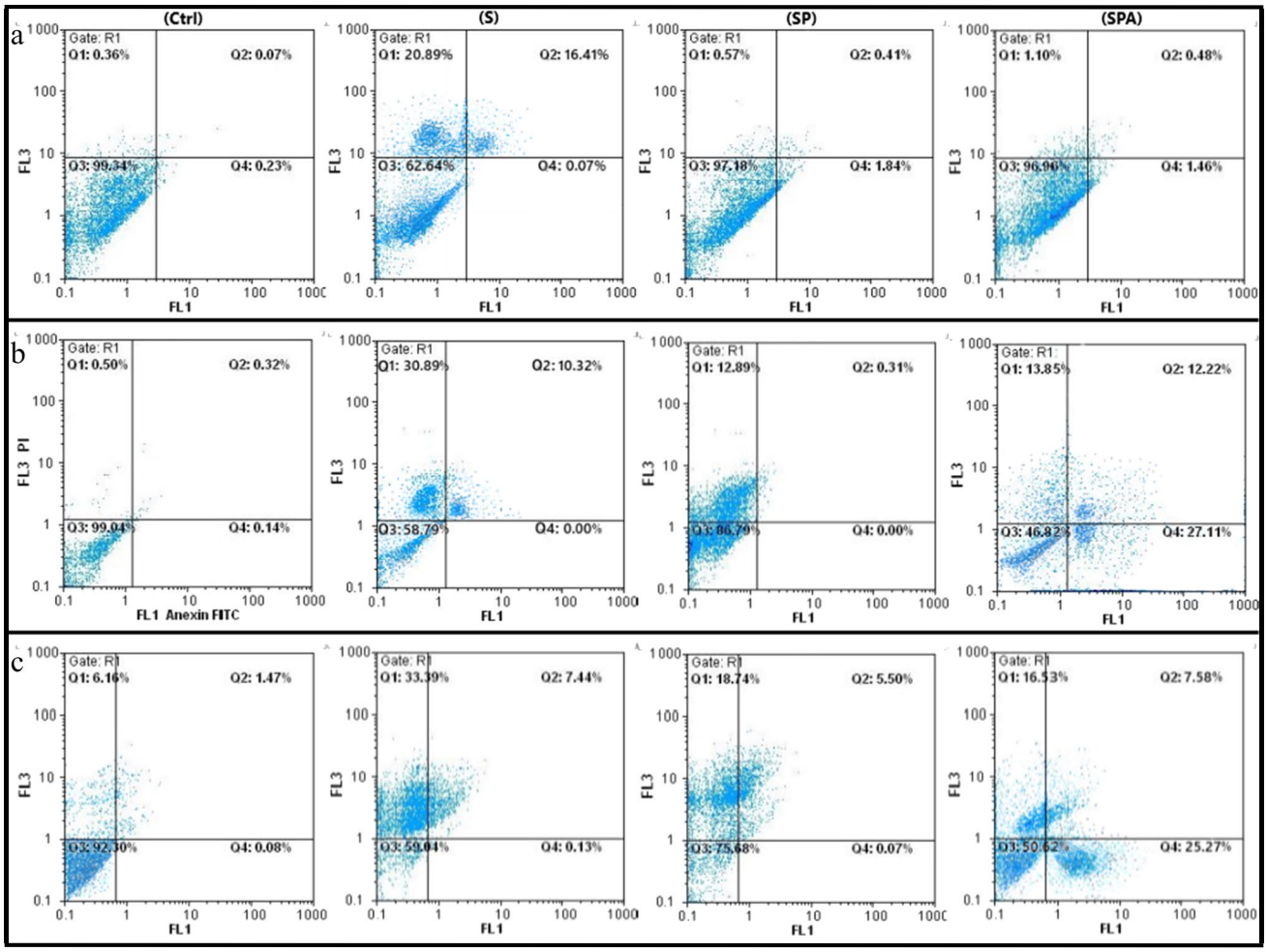

Fig. 8 Apoptosis induction in the cell lines was treated with free SBN (S), SBN-PLGA (F5) NPs (SP), and SBN-PLGA-5TR1 (F5-5TR1) nanocomplex (SPA) for 48 h and analyzed using flow cytometry. The dose of SBN in all treatment groups was constant based on the IC_{50} of free SBN in each cell line. The Ctrl group is the cells without treatments. Row **a** Apoptosis results in the CHO cells (normal cells), Row **b** Apoptosis results in the C26 cells (murine CRC cells), and Row **c** Apoptosis results in the HT29 cells (human CRC cells) (n=3)

physically integrated into the PLGA NPs without any chemical interaction between the drug and the matrix in the optimum formulation.

DSC offers information about the physical attributes and thermal features of the samples [79]. The DSC thermogram of SBN-PLGA NPs showed the absence of the distinctive endothermic melting peak of SBN (Figure 3). The findings suggest that SBN was encapsulated and likely transformed into an amorphous state inside the polymeric matrix [75].

According to the stability test results (Table II), SBN-PLGA NPs stored at both temperatures maintained a consistent nanometer size range. No significant changes in size, PDI, EE%, and ZP were observed ($P>0.05$), indicating that storing SBN-PLGA NPs at 4 and 25 °C might be appropriate. Therefore, our SBN-PLGA formulation is stable enough to be stored in freeze-dried form and rehydrated prior to use. Polymeric NPs have shown the capacity to enhance medication stability by shielding them from degradation and environmental influences that might affect treatment effectiveness. Additionally, they can improve the physical properties of pharmaceuticals [55, 80].

According to the *in vitro* release test, it was noted that there was no significant immediate release, possibly due to the encapsulation of all the drugs within the polymeric matrix which offered an extended-release profile (Figure 5). Similar drug release profiles were observed in previous studies on etodolac-loaded PLGA NPs and minocycline-loaded PLGA NPs [81, 82]. After being dispersed in the release media, the nanocomplex underwent slow dissolution of the PLGA, resulting in the formation of cavities or the release of the medication through disintegration. The dense structure of the polymer matrix and coating around the drug helps to maintain its sustained release pattern [83]. Due to a significant increase in drug release at pH 5.5 compared to neutral

pH, it is expected that the SBN-PLGA-5TR1 nanocomplex may efficiently release drugs in the acidic endosomes and lysosomes of CRC cells and facilitate the targeting of SBN to the cell nucleus [84].

Another factor to consider is the molecular weight of a polymer which plays a significant role in the release mechanism. It's a reflection of the polymer's chain length, with higher molecular weights indicating longer chains. Additionally, the chain length influences the polymer's hydrophilicity or lipophilicity. A decrease in chain length reduces lipophilicity and accelerates the polymer's degradation rate [85]. In our study, we utilized low molecular weight acid-terminated PLGA (7000-17000 Da). We hypothesize that degradation is the primary determinant of release rate in low molecular weight PLGAs [38]. This degradation rate varies and intensifies over time, resulting in a constant release rate, known as zero order release. The degradation rate's increase over time can be attributed to autocatalysis and the polymer's glass transition temperature (T_g). The presence of acidic monomers and oligomers, containing carboxylic acid end groups, speeds up the degradation process, leading to an accelerated deterioration rate. The T_g of a polymer decreases as its molecular weight decreases, making the polymer more susceptible to water absorption – the plasticizing effect of water. This decrease in T_g allows the polymer chain segments to become more mobile and prone to breakdown [86].

The primary limitation in employing free SBN for CRC treatment is its poor water solubility, hindering its bioavailability. PLGA NPs have emerged as a promising solution for drug delivery to tumor sites. These NPs protect poorly soluble and unstable payloads from the biological environment and are tiny enough, to enable capillary penetration, internalization, and endosomal escape. Furthermore, their surface modification allows for targeted delivery of SBN to CRC cells [87].

According to the *in vitro* cytotoxicity assay (Figure 6), blank PLGA NPs, and 5TR1 Apt did not reduce the viability of the tested cell lines, demonstrating the biocompatibility of PLGA as a carrier for nanosystem drug delivery and 5TR1 as a targeting agent. Also, due to the negligible release of SBN from PLGA NPs in the neutral pH environment of CHO cells, almost complete recovery of them was observed in the SP group with high viability. The effect of a produced nanocomplex on cell viability was also assessed, showing limited interaction with normal CHO cells due to the absence of MUC1 receptors for 5TR1 Apt [52]. The addition of 5TR1 Apt to SBN-PLGA notably enhanced the antiproliferative effect of free and encapsulated SBN, as the 5TR1 Apt strongly attracted to the MUC1 receptors on the C26 and HT29 cell membranes, leading to uptake of the nanocomplex by CRC cells.

While some prior research has employed nanocomplexes containing 5TR1 to alleviate the negative impact of drugs on healthy cells, this study was the first effort to utilize the 5TR1 as a probe for the targeted delivery of a natural agent (SBN) to CRC cells, using PLGA NPs as the carrier. Also, there are a few efforts on SBN delivery with nano carriers for cancer treatment and all of them are passive delivery with possible invasive cytotoxic effects. In one study a co-delivery of SBN and cryptotanshinone with lipid-polymeric hybrid NPs was performed against the metastatic breast cancer. The hybrid NPs enhance drug penetration across intestinal barriers, increasing oral bioavailability. They also show anti-metastatic properties in mice with breast cancer [88]. In a separate study, SBN-conjugated gold NPs improve the effectiveness of SBN in eliminating lung cancer cells by 4-5 fold [89]. In this research we found that 5TR1 Apt specifically targeted MUC1-positive cell lines (C26 and HT29), delivering the SBN to the CRC cells and protecting non-target cells (CHO) from SBN-induced cell death. This suggests that Apt probes have the potential for precise targeting of CRC cells while minimizing harm to healthy cells. Additionally, the use of PLGA NPs as a carrier ensures regulated drug administration to the targeted area and prolongs its presence in the bloodstream [90, 91]. The higher cytotoxicity of free SBN compared to the SBN-PLGA NPs is attributed to the sustained release profile of the drug from the polymeric matrix. Nevertheless, the current investigation indicates that using Apt and PLGA NPs might significantly enhance the selectivity of an anti-cancer medication (SBN) for CRC therapy.

Apoptosis is a crucial process in both normal biological functions and numerous cell-related diseases. It may be triggered by several events, all leading to a planned and organized cell death. One technique used to investigate apoptosis involves detecting changes in the localization of phosphatidylserine (PS) inside the cellular membrane. Within non-apoptotic cells, the majority of PS molecules are situated on the inner surface of the plasma membrane. However, during the early stages of apoptosis, PS is repositioned to the outer surface of the membrane, therefore becoming accessible to the external environment [92]. Annexin V, a 35.8-kDa protein, may readily identify exposed PS due to its high affinity for PS.

The proportion of apoptotic and dead cells was evaluated by Annexin V-FITC/PI staining. Figure 8 demonstrates that when C26 and HT29 cell lines are exposed to SBN-PLGA-5TR1 nanocomplex, there is a promotion of phosphatidylserine translocation from the inner membrane of the cells to the outer membrane surface. This translocation can be identified by Annexin V and is likely caused by apoptosis-related processes [39]. Both the C26 and HT29 cell lines exhibited significant indications of apoptosis in cells treated with the SBN-PLGA-5TR1 nanocomplex ($P<0.0001$). Another advantage of this nanocomplex is its noninvasive and non-cytotoxicity effect on normal cell line (CHO) which

is supported by the MTT assay results. Neither SBN-PLGA NPs nor the SBN-PLGA-5TR1 nanocomplex led to cell death when compared to free SBN. These observations could be due to the negligible release of SBN from SBN-PLGA NPs in physiologic pH (7.4) (Figure 5) and the absence of MUC1 on the surface of CHO cells. Emerging research indicates that SBN has the potential to directly diminish cell viability in several types of cancers, such as those found in the skin, bladder, colon, prostate, lung, and breast [9, 93, 94]. Also, PLGA NPs could passively target the CRC cells. But, based on our findings the main mechanism associated with free SBN and SBN-PLGA NPs for anti-cancer activity is necrotic death which causes the release of proinflammatory intracellular contents and affects the surrounding healthy tissues [95]. Nejabati et al. developed a 5TR1-modified PLGA NPs to combine doxorubicin (DOX) and SmacN6 (an antagonist of the IAPs) in a treatment targeting CRC cells (C26 cell line). The Western blot analysis confirmed the mechanism by which cell death occurs, including the activation of caspases via both intrinsic and extrinsic pathways. This process is related to the 5TR1-modified PLGA NPs [96]. Furthermore, the data validate the hypothesis that the enhanced endocytosis of 5TR1-nanocomplex to the CRC cells (C26 and HT29) is associated with the connection between cell growth and apoptosis.

The authors encountered several limitations during this study. Notably, the stability evaluation period may not have fully captured the longer-term stability of the SBN-PLGA NPs. Furthermore, this study only evaluated the developed nanocomplex using in vitro cell culture models. While this work provided valuable insights into cellular uptake, cytotoxicity, and targeting capability, the results may not fully translate to *in vivo* performance and efficacy. Additional studies in animal models would be needed to assess the NPs' biodistribution, pharmacokinetics, and therapeutic effectiveness in a more physiologically relevant system. Lastly, the current study only focuses on *in vitro* cytotoxicity and does not investigate potential systemic toxicities or side effects of the nanocomplex. Conducting *in vivo* toxicology studies would be an important next step to fully characterize this drug delivery system's safety profile. Overall, this in vitro study demonstrated promising results. However, more comprehensive research is needed to thoroughly evaluate the therapeutic potential and limitations of the SBN-loaded, Apt-decorated PLGA NPs for CRC treatment.

Conclusion

In summary, the authors have developed a platform for the delivery of SBN to CRC cells through the encapsulation of this substance in PLGA NPs and the use of the 5TR1 Apt to selectively bind the NPs to target cells (HT29 and C26 cells). The SBN-PLGA NPs that were generated demonstrated excellent SBN entrapment and pH sensitivity. The findings of this research provided evidence for the effectiveness of the SBN-PLGA-5TR1 nanocomplex in inhibiting cell proliferation in HT29 and C26 cells. In addition, Annexin V-FITC/PI staining supported the antitumor properties of the developed nanocomplex. The findings suggest that the SBN-PLGA-5TR1 nanocomplex can serve as a delivery system, offering a potentially effective approach to enhance the anticancer properties of SBN without the need for any chemotherapy drugs. Overall, the future of SBN-PLGA-5TR1 nanocomplex for CRC treatment is promising, with advancements focused on improving delivery systems, adopting a multi-targeted approach, incorporating natural ingredients, ensuring biocompatibility and safety, offering personalized solutions, and complying with regulatory requirements. These findings provide a foundation for developing novel and efficacious anticancer strategies that address diverse consumer demands while adhering to stringent efficacy and safety criteria. Given the promising *in vitro* anticancer potential of the nanocomplex, further *in vivo* studies are warranted to evaluate its pharmacokinetics and antitumor efficacy and establish its potential as a novel therapeutic approach for CRC patients.

Abbreviations **ANOVA**: Analysis of Variance; **Apt**: Aptamer; **ATR-FTIR**: Attenuated Total Reflectance-Fourier Transform Infrared; **C26**: Murine colorectal carcinoma cell line; **CHO**: Chinese Hamster Ovary cell line; **CRC**: Colorectal Cancer; **DMSO**: Dimethyl Sulfoxide; **DLS**: Dynamic Light Scattering; **DOX**: Doxorubicin; **DSC**: Differential Scanning Calorimetry; **EDC**: 1-ethyl-3-(3-dimethylaminopropyl) carbodiimide hydrochloride; **EE**: Entrapment Efficiency; **EGFR**: Epidermal Growth Factor Receptor; **ELISA**: Enzyme-Linked Immunosorbent Assay; **EPR**: Enhanced Permeability and Retention; **FBS**: Fetal Bovine Serum; **FE-SEM**: Field Emission Scanning Electron Microscopy; **HT29**: Human colorectal adenocarcinoma cell line; **ICH**: International Council for Harmonization; **MUC1**: Mucin 1; **NHS**: N-hydroxy sulfosuccinimide; **NP**: Nanoparticle; **PBS**: Phosphate-buffered Saline; **PDI**: Polydispersity Index; **Pen/Strep**: Penicillin–Streptomycin; **PI**: Propidium Iodide; **PLGA**: Poly (lactic-co-glycolic acid); **SBN**: Silybin or Silibinin; **SD**: Standard Deviation; **SELEX**: Systematic Evolution of Ligands by Exponential Enrichment; **ZP**: Zeta Potential

Authors' Contributions Seyyed Mobin Rahimnia was responsible for writing the original draft, methodology and investigation, data analysis, reviewing, and editing the manuscript. Majid Saeedi was responsible for the supervision, conceptualization, reviewing, and editing of the manuscript. Jafar Akbari was responsible for the supervision and data analysis. Katayoun Morteza-Semnani was responsible for the supervision and data analysis. Akbar Hedayatizadeh-Omran was responsible for reviewing, and editing the manuscript. Rezvan Yazdian-Robati was responsible for the conceptualization, supervision, data analysis, reviewing, and editing of the manuscript.

Funding The current study has been financially supported by the research council at Mazandaran University of Medical Sciences under grant number 11850.

Data Availability The data used and/or examined in the current work could be obtained upon a reasonable request.

Declarations

Ethics Approval Approval for all experiments was granted by the ethics committee of Mazandaran University of Medical Sciences under registration code IR.MAZUMS.REC.1401.11850.

Conflicts of Interest The current research has not encountered any conflict of interest.

References

1. Siegel RL, Wagle NS, Cercek A, Smith RA, Jemal A. Colorectal cancer statistics, 2023. CA: A Cancer J Clin. 2023;73(3):233–54.
2. Alzahrani SM, Al Doghaither HA, Al-Ghafari AB, Pushparaj PN. 5-Fluorouracil and capecitabine therapies for the treatment of colorectal cancer. Oncol Reports. 2023;50(4):1–16.
3. Blondy S, David V, Verdier M, Mathonnet M, Perraud A, Christou N. 5-Fluorouracil resistance mechanisms in colorectal cancer: From classical pathways to promising processes. Cancer Sci. 2020;111(9):3142–54.
4. Deschoolmeester V, Smits E, Peeters M, Vermorken JB. Status of active specific immunotherapy for stage II, stage III, and resected stage IV colon cancer. Curr Colorectal Cancer Reports. 2013;9:380–90.
5. Siegel RL, Miller KD, Jemal A. Cancer statistics, 2015. CA: A Cancer J Clin. 2015;65(1):5–29.
6. Hashemi M, Shamshiri A, Saeedi M, Tayebi L, Yazdian-Robati R. Aptamer-conjugated PLGA nanoparticles for delivery and imaging of cancer therapeutic drugs. Arch Biochem Biophys. 2020;691:108485.
7. Vargas-Mendoza N, Madrigal-Santillán E, Morales-González Á, Esquivel-Soto J, Esquivel-Chirino C, y González-Rubio MG-L, et al. Hepatoprotective effect of silymarin. World journal of hepatology. 2014;6(3):144.
8. Wang Y, Yuan A-J, Wu Y-J, Wu L-M, Zhang L. Silymarin in cancer therapy: Mechanisms of action, protective roles in chemotherapy-induced toxicity, and nanoformulations. J Funct Foods. 2023;100:105384.
9. Deep G, Agarwal R. Antimetastatic efficacy of silibinin: molecular mechanisms and therapeutic potential against cancer. Cancer Metastasis Rev. 2010;29:447–63.
10. Hoh C, Boocock D, Marczylo T, Singh R, Berry DP, Dennison AR, et al. Pilot study of oral silibinin, a putative chemopreventive agent, in colorectal cancer patients: silibinin levels in plasma, colorectum, and liver and their pharmacodynamic consequences. Clin Cancer Res. 2006;12(9):2944–50.
11. Flaig TW, Gustafson DL, Su L-J, Zirrolli JA, Crighton F, Harrison GS, et al. A phase I and pharmacokinetic study of silybin-phytosome in prostate cancer patients. Investig New Drugs. 2007;25:139–46.
12. Flaig TW, Glodé M, Gustafson D, van Bokhoven A, Tao Y, Wilson S, et al. A study of high-dose oral silybin-phytosome followed by prostatectomy in patients with localized prostate cancer. The Prostate. 2010;70(8):848–55.
13. Vazhappilly CG, Amararathna M, Cyril AC, Linger R, Matar R, Merheb M, et al. Current methodologies to refine bioavailability, delivery, and therapeutic efficacy of plant flavonoids in cancer treatment. J Nutr Biochem. 2021;94:108623.
14. Wei Y, Ye X, Shang X, Peng X, Bao Q, Liu M, et al. Enhanced oral bioavailability of silybin by a supersaturatable self-emulsifying drug delivery system (S-SEDDS). Colloids Surf A: Physicochem Eng Asp. 2012;396:22–8.
15. Yazdian-Robati R, Ramezani M, Jalalian SH, Abnous K, Taghdisi SM. Targeted delivery of epirubicin to cancer cells by polyvalent aptamer system *in vitro* and *in vivo*. Pharm Res. 2016;33:2289–97.
16. Danhier F, Ansorena E, Silva JM, Coco R, Le Breton A, Préat V. PLGA-based nanoparticles: an overview of biomedical applications. J Control Release. 2012;161(2):505–22.
17. Jahan ST, Sadat SM, Walliser M, Haddadi A. Targeted therapeutic nanoparticles: an immense promise to fight against cancer. J Drug Deliv. 2017;2017(1):9090325.
18. Betancourt T, Byrne JD, Sunaryo N, Crowder SW, Kadapakkam M, Patel S, et al. PEGylation strategies for active targeting of PLA/PLGA nanoparticles. J Biomed Mater Res Part A: An Off J Soc Biomater, The Japanese Soc Biomater, and The Australian Soc Biomater and the Korean Soc Biomater. 2009;91(1):263–76.
19. Chiu HI, Samad NA, Fang L, Lim V. Cytotoxicity of targeted PLGA nanoparticles: A systematic review. RSC adv. 2021;11(16):9433–49.
20. Zhang D, Liu L, Wang J, Zhang H, Zhang Z, Xing G, et al. Drug-loaded PEG-PLGA nanoparticles for cancer treatment. Front Pharmacol. 2022;13:990505. https://doi.org/10.3389/fphar.2022.990505.
21. Derman S, Mansuroglu B, Bozkurt Y, Tayfun A, POYRAZ FS. Drug comprising plga nanoparticles loaded with cape targeted with angiopep-2 peptide. United States patent, US20230225983A1; 2023.
22. Sharma P, Kaur N, Shanavas A. Chapter 5 - Targeting strategies using PLGA nanoparticles for efficient drug delivery. In: Kesharwani P, editor. Poly(lactic-co-glycolic acid) (PLGA) Nanoparticles for Drug Delivery. Elsevier; 2023. p. 123–51.
23. Abamor ES, Allahverdiyev A, Tosyali OA, Bagirova M, Acar T, Mustafaeva Z, et al. Evaluation of in vitro and *in vivo* immunostimulatory activities of poly (lactic-co-glycolic acid) nanoparticles loaded with soluble and autoclaved Leishmania infantum antigens: a novel vaccine candidate against visceral leishmaniasis. Asian Pac J Trop Med. 2019;12(8):353–64.
24. Ucar B, Acar T, Arayici PP, Derman S. A nanotechnological approach in the current therapy of COVID-19: model drug oseltamivir-phosphate loaded PLGA nanoparticles targeted with spike protein binder peptide of SARS-CoV-2. Nanotechnology. 2021;32(48):485601.
25. Vanderhoff JW, El-Aasser MS, Ugelstad J. Polymer emulsification process. United States patent, US4177177A; 1979.
26 Nava-Arzaluz MG, Piñón-Segundo E, Ganem-Rondero A, Lechuga-Ballesteros D. Single emulsion-solvent evaporation technique and modifications for the preparation of pharmaceutical polymeric nanoparticles. Recent Patents Drug Deliv Formulation. 2012;6(3):209–23.
27. Han J, Gao L, Wang J, Wang J. Application and development of aptamer in cancer: from clinical diagnosis to cancer therapy. J Cancer. 2020;11(23):6902.
28. Farokhzad OC, Karp JM, Langer R. Nanoparticle–aptamer bioconjugates for cancer targeting. Expert Opin Drug Deliv. 2006;3(3):311–24.
29. Shahdordizadeh M, Yazdian-Robati R, Ramezani M, Abnous K, Taghdisi SM. Aptamer application in targeted delivery systems for diagnosis and treatment of breast cancer. J Mater Chem B. 2016;4(48):7766–78.
30. Gao G, Liu C, Jain S, Li D, Wang H, Zhao Y, et al. Potential use of aptamers for diagnosis and treatment of pancreatic cancer. J Drug Target. 2019;27(8):853–65.
31. Nabavinia MS, Gholoobi A, Charbgoo F, Nabavinia M, Ramezani M, Abnous K. Anti-MUC1 aptamer: a potential opportunity for cancer treatment. Med Res Rev. 2017;37(6):1518–39.

32. Yazdian-Robati R, Bayat P, Dehestani S, Hashemi M, Taghdisi SM, Abnous K. Smart delivery of epirubicin to cancer cells using aptamer-modified ferritin nanoparticles. J Drug Target. 2022;30(5):567–76.
33. Kızılbey K. Optimization of rutin-loaded PLGA nanoparticles synthesized by single-emulsion solvent evaporation method. Acs Omega. 2019;4(1):555–62.
34. Shahabadi N, Moshiri M, Roohbakhsh A, Imenshahidi M, Hashemi M, Amin F, et al. A dose-related positive effect of inhaled simvastatin-loaded PLGA nanoparticles on paraquat-induced pulmonary fibrosis in rats. Basic Clin Pharmacol Toxicol. 2022;131(4):251–61.
35. Ebrahimian M, Shahgordi S, Yazdian-Robati R, Etemad L, Hashemi M, Salmasi Z. Targeted delivery of galbanic acid to colon cancer cells by PLGA nanoparticles incorporated into human mesenchymal stem cells. Avicenna J Phytomed. 2022;12(3):295.
36. Tripathi A, Gupta R, Saraf SA. PLGA nanoparticles of anti tubercular drug: drug loading and release studies of a water in-soluble drug. Int J Pharm Tech Res. 2010;2(3):2116–23.
37. Yuan X, Ji W, Chen S, Bao Y, Tan S, Lu S, et al. A novel paclitaxel-loaded poly (d, l-lactide-co-glycolide)-Tween 80 copolymer nanoparticle overcoming multidrug resistance for lung cancer treatment. Int J Nanomedicine. 2016;11:2119–31.
38. Mittal G, Sahana D, Bhardwaj V, Kumar MR. Estradiol loaded PLGA nanoparticles for oral administration: effect of polymer molecular weight and copolymer composition on release behavior *in vitro* and *in vivo*. J Control Release. 2007;119(1):77–85.
39. Esim O, Bakirhan NK, Sarper M, Savaser A, Ozkan SA, Ozkan Y. Influence of emulsifiers on the formation and in vitro anticancer activity of epirubicin loaded PLGA nanoparticles. J Drug Deliv Sci Technol. 2020;60:102027.
40. Khoee S, Yaghoobian M. An investigation into the role of surfactants in controlling particle size of polymeric nanocapsules containing penicillin-G in double emulsion. European J Med Chem. 2009;44(6):2392–9.
41. Sharma N, Madan P, Lin S. Effect of process and formulation variables on the preparation of parenteral paclitaxel-loaded biodegradable polymeric nanoparticles: A co-surfactant study. Asian J Pharm Sci. 2016;11(3):404–16.
42. Saeedi M, Morteza-Semnani K, Akbari J, Hajheydari Z, Goodarzi A, Rostamkalaei SS, et al. Green formulation of spironolactone loaded chitosan-coated nano lipid carrier for treatment of acne vulgaris: A randomized double-blind clinical trial. Adv Pharm Bull. 2024;14(1):161.
43. Bakhshi F, Molavi O, Rashidi MR, Shayanfar A, Amini H. Developing a high-performance liquid chromatography fast and accurate method for quantification of silibinin. BMC Res Notes. 2019;12(1):1–6.
44. Gatabi ZR, Saeedi M, Morteza-Semnani K, Rahimnia SM, Yazdian-Robati R, Hashemi SMH. Green preparation, characterization, evaluation of anti-melanogenesis effect and *in vitro/in vivo* safety profile of kojic acid hydrogel as skin lightener formulation. J Biomater Sci Polym Ed. 2022;33(17):2270–91.
45. Saeedi M, Morteza-Semnani K, Akbari J, Rahimnia SM, Babaei A, Eghbali M, et al. Eco-friendly preparation, characterization, evaluation of anti-melanogenesis/antioxidant effect and in vitro/in vivo safety profile of kojic acid loaded niosome as skin lightener preparation. J Biomater Sci Polym Ed. 2023;34(14):1952–80.
46. Saeedi M, Morteza-Semnani K, Siahposht-Khachaki A, Akbari J, Valizadeh M, Sanaee A, et al. Passive targeted drug delivery of venlafaxine hcl to the brain by modified chitosan nanoparticles: Characterization, cellular safety assessment, and in vivo evaluation. J Pharm Innov. 2023;18(3):1441–53.
47. Rahimnia SM, Saeedi M, Morteza-Semnani K, Akbari J, Ghasemi M, Abootorabi S, et al. Green preparation, characterization, wound healing assessment, and histopathological evaluation of Vitamin A encapsulated in niosome and solid lipid nanoparticle. Pharm Sci. 2023;30(1):70–84.
48. Alibolandi M, Ramezani M, Abnous K, Hadizadeh F. AS1411 aptamer-decorated biodegradable polyethylene glycol–poly (lactic-co-glycolic acid) nanopolymersomes for the targeted delivery of gemcitabine to non–small cell lung cancer in vitro. J Pharm Sci. 2016;105(5):1741–50.
49. Vyas A, Kumar Sonker A, Gidwani B. Carrier-based drug delivery system for treatment of acne. Sci World J. 2014;2014.
50. Paswan SK, Saini T. Comparative evaluation of in vitro drug release methods employed for nanoparticle drug release studies. Clin Trials. 2021;14:17.
51. Durymanov M, Permyakova A, Reineke J. Pre-treatment with PLGA/silibinin nanoparticles mitigates dacarbazine-induced hepatotoxicity. Front Bioeng Biotechnol. 2020;8:495.
52. Taghavi S, Ramezani M, Alibolandi M, Abnous K, Taghdisi SM. Chitosan-modified PLGA nanoparticles tagged with 5TR1 aptamer for *in vivo* tumor-targeted drug delivery. Cancer Lett. 2017;400:1–8.
53. Taleghani AS, Ebrahimnejad P, Heydarinasab A, Akbarzadeh A. Adsorption and controlled release of iron-chelating drug from the amino-terminated PAMAM/ordered mesoporous silica hybrid materials. J Drug Deliv Sci Technol. 2020;56:101579.
54. Afsharzadeh M, Abnous K, Yazdian-Robati R, Ataranzadeh A, Ramezani M, Hashemi M. Formulation and evaluation of anticancer and antiangiogenesis efficiency of PLA–PEG nanoparticles loaded with galbanic acid in C26 colon carcinoma, in vitro and *in vivo*. J Cell Physiol. 2019;234(5):6099–107.
55. Saeedi M, Morteza-Semnani K, Akbari J, Rahimnia SM, Ahmadi F, Choubdari H, et al. Development of kojic acid loaded collagen-chitosan nanoparticle as skin lightener product: *in vitro* and *in vivo* assessment. J Biomater Sci Polym Ed. 2024;35(1):63–84.
56. Yazdian-Robati R, Amiri E, Kamali H, Khosravi A, Taghdisi SM, Jaafari MR, et al. CD44-specific short peptide A6 boosts cellular uptake and anticancer efficacy of PEGylated liposomal doxorubicin *in vitro* and *in vivo*. Cancer Nanotechnol. 2023;14(1):84.
57. Hogan FS, Krishnegowda NK, Mikhailova M, Kahlenberg MS. Flavonoid, silibinin, inhibits proliferation and promotes cell-cycle arrest of human colon cancer. J Surg Res. 2007;143(1):58–65.
58. Hashemi M, Abnous K, Balarastaghi S, Hedayati N, Salmasi Z, Yazdian-Robati R. Mitoxantrone-loaded PLGA nanoparticles for increased sensitivity of glioblastoma cancer cell to TRAIL-induced apoptosis. J Pharm Innov. 2022;17:207–14.
59. Sahibzada MUK, Sadiq A, Khan S, Faidah HS, Naseemullah, Khurram M, et al. Fabrication, characterization and in vitro evaluation of silibinin nanoparticles: an attempt to enhance its oral bioavailability. Drug Des Dev Ther. 2017;1453-64.
60. Pirooznia N, Hasannia S, Lotfi AS, Ghanei M. Encapsulation of alpha-1 antitrypsin in PLGA nanoparticles: in vitro characterization as an effective aerosol formulation in pulmonary diseases. J Nanobiotechnol. 2012;10(1):1–15.
61. Campos M, Fialho SL, Pereira BG, Yoshida MI, Mussel W, Junior A, et al. Development and chemical characterization of biodegradable polymeric implants containing sirolimus for the treatment of malignant solid tumors. Die Pharmazie-An Int J Pharm Sci. 2019;74(4):221–6.
62. Hashemi M, Haghgoo Z, Yazdian-Robati R, Shahgordi S, Salmasi Z, Abnous K. Improved anticancer efficiency of Mitoxantrone by Curcumin loaded PLGA nanoparticles targeted with AS1411 aptamer. Nanomed J. 2021;8(1).
63. Yu C, Hu Y, Duan J, Yuan W, Wang C, Xu H, et al. Novel aptamer-nanoparticle bioconjugates enhances delivery of anticancer drug to MUC1-positive cancer cells in vitro. PloS one. 2011;6(9):e24077.

64. Raj R, Mongia P, Ram A, Jain N. Enhanced skin delivery of aceclofenac via hydrogel-based solid lipid nanoparticles. Artif Cells, Nanomed, Biotechnol. 2016;44(6):1434–9.
65. Rowe RC, Sheskey PJ, Owen SC. Handbook of pharmaceutical excipients. 5th ed. American Pharmacists Association: Pharmaceutical Press; 2006.
66 Mitchell DJ, Ninham BW. Micelles, vesicles and microemulsions. J Chem Soc, Faraday Trans 2 Mol Chem Phys. 1981;77(4):601–29.
67. Winzenburg G, Schmidt C, Fuchs S, Kissel T. Biodegradable polymers and their potential use in parenteral veterinary drug delivery systems. Adv Drug Deliv Rev. 2004;56(10):1453–66.
68. Azizi M, Farahmandghavi F, Joghataei M, Zandi M, Imani M, Bakhtiary M, et al. Fabrication of protein-loaded PLGA nanoparticles: effect of selected formulation variables on particle size and release profile. J Polym Res. 2013;20:1–14.
69. Akbari J, Saeedi M, Morteza-Semnani K, Ghasemi M, Eshaghi M, Eghbali M, et al. An eco-friendly and hopeful promise platform for delivering hydrophilic wound healing agents in topical administration for wound disorder: diltiazem-loaded niosomes. J Pharm Innov. 2023;18(1):1111–27.
70. Kharia AA, Singhai A, Verma R. Formulation and evaluation of polymeric nanoparticles of an antiviral drug for gastroretention. Int J Pharm Sci Nanotechnol. 2012;4(4):1557–62.
71. Sabbah M, Esposito M, Pierro PD, Giosafatto C, Mariniello L, Porta R. Insight into zeta potential measurements in biopolymer film preparation. J Biotechnol Biomater. 2016;6(2):2–4.
72. Xie S, Wang S, Zhao B, Han C, Wang M, Zhou W. Effect of PLGA as a polymeric emulsifier on preparation of hydrophilic protein-loaded solid lipid nanoparticles. Coll Surf B: Biointerfaces. 2008;67(2):199–204.
73. Sun S-B, Liu P, Shao F-M, Miao Q-L. Formulation and evaluation of PLGA nanoparticles loaded capecitabine for prostate cancer. Int J Clin Exp Med. 2015;8(10):19670.
74. Shah R, Eldridge D, Palombo E, Harding I. Optimisation and stability assessment of solid lipid nanoparticles using particle size and zeta potential. J Phys Sci. 2014;25(1).
75. Mu L, Feng S. A novel controlled release formulation for the anticancer drug paclitaxel (Taxol®): PLGA nanoparticles containing vitamin E TPGS. J Control Release. 2003;86(1):33–48.
76. Ma N, Ma C, Li C, Wang T, Tang Y, Wang H, et al. Influence of nanoparticle shape, size, and surface functionalization on cellular uptake. J Nanosci Nanotechnol. 2013;13(10):6485–98. https://doi.org/10.1166/jnn.2013.7525.
77. Saeedi M, Morteza-Semnani K, Akbari J, Hajheydari Z, Goodarzi A, Rostamkalaei SS, et al. Green formulation of spironolactone loaded chitosan coated nano lipid carrier for treatment of acne vulgaris: a randomized double-blind clinical trial. Adv Pharm Bullet. 2023;14(1):161–75.
78. Rybak-Smith MJ, Tripisciano C, Borowiak-Palen E, Lamprecht C, Sim RB. Effect of functionalization of carbon nanotubes with psychosine on complement activation and protein adsorption. J Biomed Nanotechnol. 2011;7(6):830–9.
79. Clas S-D, Dalton CR, Hancock BC. Differential scanning calorimetry: applications in drug development. Pharm Sci Technol Today. 1999;2(8):311–20.
80. Aryal S, Hu C-MJ, Zhang L. Polymer– cisplatin conjugate nanoparticles for acid-responsive drug delivery. ACS nano. 2010;4(1):251–8.
81. Çırpanlı Y, Robineau C, Çapan Y, Çalış S. Etodolac Loaded Poly Lactide-Co-Glycolide Nanoparticles: Formulation and In Vitro Characterization. Hacet Univ J Fac Pharm. 2009;2:105–14.
82. Kashi TSJ, Eskandarion S, Esfandyari-Manesh M, Marashi SMA, Samadi N, Fatemi SM, et al. Improved drug loading and antibacterial activity of minocycline-loaded PLGA nanoparticles prepared by solid/oil/water ion pairing method. Int J Nanomed. 2012;7(1):221–34.
83. Venkatesh DN, Baskaran M, Karri VVSR, Mannemala SS, Radhakrishna K, Goti S. Fabrication and *in vivo* evaluation of Nelfinavir loaded PLGA nanoparticles for enhancing oral bioavailability and therapeutic effect. Saudi Pharm J. 2015;23(6):667–74.
84. Yazdian-Robati R, Arab A, Ramezani M, Rafatpanah H, Bahreyni A, Nabavinia MS, et al. Smart aptamer-modified calcium carbonate nanoparticles for controlled release and targeted delivery of epirubicin and melittin into cancer cells *in vitro* and *in vivo*. Drug Dev Indust Pharm. 2019;45(4):603–10.
85. Jain RA. The manufacturing techniques of various drug loaded biodegradable poly (lactide-co-glycolide)(PLGA) devices. Biomaterials. 2000;21(23):2475–90.
86. Park TG. Degradation of poly (D, L-lactic acid) microspheres: effect of molecular weight. J Control Release. 1994;30(2):161–73.
87. Tabatabaei Mirakabad FS, Nejati-Koshki K, Akbarzadeh A, Yamchi MR, Milani M, Zarghami N, et al. PLGA-based nanoparticles as cancer drug delivery systems. Asian Pac J Cancer Prev. 2014;15(2):517–35.
88. Liu Y, Xie X, Hou X, Shen J, Shi J, Chen H, et al. Functional oral nanoparticles for delivering silibinin and cryptotanshinone against breast cancer lung metastasis. J Nanobiotechnol. 2020;18(1):1–15.
89. Ravi R, Zeyaullah M, Ghosh S, Khan Warsi M, Baweja R, AlShahrani AM, et al. Use of gold nanoparticle-silibinin conjugates: A novel approach against lung cancer cells. Front Chem. 2022;10:1018759.
90. Graf N, Bielenberg DR, Kolishetti N, Muus C, Banyard J, Farokhzad OC, et al. αVβ3 integrin-targeted PLGA-PEG nanoparticles for enhanced anti-tumor efficacy of a Pt (IV) prodrug. ACS Nano. 2012;6(5):4530–9.
91. Tang Y, Lei T, Manchanda R, Nagesetti A, Fernandez-Fernandez A, Srinivasan S, et al. Simultaneous delivery of chemotherapeutic and thermal-optical agents to cancer cells by a polymeric (PLGA) nanocarrier: an in vitro study. Pharm Res. 2010;27:2242–53.
92. Martin S, Reutelingsperger C, McGahon AJ, Rader JA, Van Schie R, LaFace DM, et al. Early redistribution of plasma membrane phosphatidylserine is a general feature of apoptosis regardless of the initiating stimulus: inhibition by overexpression of Bcl-2 and Abl. J Exp Med. 1995;182(5):1545–56.
93. Agarwal C, Wadhwa R, Deep G, Biedermann D, Gažák R, Křen V, et al. Anti-cancer efficacy of silybin derivatives-a structure-activity relationship. PLoS One. 2013;8(3):e60074.
94. Deep G, Agarwal R. Chemopreventive efficacy of silymarin in skin and prostate cancer. Integr Cancer Ther. 2007;6(2):130–45.
95. Patel VA, Longacre A, Hsiao K, Fan H, Meng F, Mitchell JE, et al. Apoptotic cells, at all stages of the death process, trigger characteristic signaling events that are divergent from and dominant over those triggered by necrotic cells: Implications for the delayed clearance model of autoimmunity. J Biol Chem. 2006;281(8):4663–70. https://doi.org/10.1074/jbc.M508342200.
96. Nejabat M, Eisvand F, Soltani F, Alibolandi M, Taghdisi SM, Abnous K, et al. Combination therapy using Smac peptide and doxorubicin-encapsulated MUC 1-targeted polymeric nanoparticles to sensitize cancer cells to chemotherapy: An *in vitro* and *in vivo* study. Int J Pharm. 2020;587:119650.